

A Pyrene–Poly(acrylic acid)–Polyrotaxane Supramolecular Binder Network for High-Performance Silicon Negative Electrodes

Yunshik Cho, Jaemin Kim, Ahmed Elabd, Sunghun Choi, Kiho Park, Tae-woo Kwon, Jungmin Lee, Kookheon Char,* Ali Coskun,* and Jang Wook Choi*

Although being incorporated in commercial lithium-ion batteries for a while, the weight portion of silicon monoxide (SiO_x , $x \approx 1$) is only less than 10 wt% due to the insufficient cycle life. Along this line, polymeric binders that can assist in maintaining the mechanical integrity and interfacial stability of SiO_x electrodes are desired to realize higher contents of SiO_x . Herein, a pyrene–poly(acrylic acid) (PAA)–polyrotaxane (PR) supramolecular network is reported as a polymeric binder for SiO_x with 100 wt%. The noncovalent functionalization of a carbon coating layer on the SiO_x is achieved by using a hydroxylated pyrene derivative via the π – π stacking interaction, which simultaneously enables hydrogen bonding interactions with the PR–PAA network through its hydroxyl moiety. Moreover, the PR's ring sliding while being crosslinked to PAA endows a high elasticity to the entire polymer network, effectively buffering the volume expansion of SiO_x and largely mitigating the electrode swelling. Based on these extraordinary physicochemical properties of the pyrene–PAA–PR supramolecular binder, the robust cycling of SiO_x electrodes is demonstrated at commercial levels of areal loading in both half-cell and full-cell configurations.

retical specific capacity ($>3000 \text{ mAh g}^{-1}$) and low operation potential ($\approx 0.3 \text{ V vs Li/Li}^+$) constitute the main advantages of Si anodes toward advanced LIBs.^[1] However, the massive volume change of Si over 300% during charging and discharging process severely impairs the structural integrity of Si electrode and consequently causes continuous decomposition of electrolyte in the electrode leading to the formation of undesirably thickened solid electrolyte interphase (SEI). This process also incurs the delamination of the electrode. It is well known that all of these detrimental phenomena jointly worsen the electrochemical performance of Si electrodes.

As for the Si particle size, nano-sized Si was mainly studied in the early stage of research due to the fact that the small particle size can more effectively release the accumulated strain during the volume change of Si and can thus withstand

Silicon (Si) is a promising anode material for next-generation Li-ion batteries (LIBs) with high energy densities. High theo-

against pulverization.^[2] However, the large surface area of nano-sized Si makes it more difficult to stabilize the SEI layer owing to its increased exposure to electrolyte, thus harming the coulombic efficiency (CE) in each cycle. Moreover, from the manufacturing viewpoint, nano-sized Si adds difficulty in maintaining uniform particle size and controlling rheological conditions of the electrode slurry. For these reasons, micrometer-size active materials such as Si-carbon blends and silicon monoxide (SiO_x , $x \approx 1$) are preferred by the industry for the cell production.^[3]

Polymeric binders have also turned out to play a crucial role in the stabilization of Si electrodes,^[4] and various concepts including 3D network structures,^[5] covalent attachment between Si and binder,^[6] hydrogen bonding interaction,^[7] ion–dipole interaction,^[8] self-healing,^[9] and molecular machines^[10] have been recently introduced. The majority of these approaches were effective in dealing with bare Si active materials by taking advantage of polar functional groups on their surface. However, commercially viable Si-carbon blends and SiO_x active materials contain carbon layers on their outer surface for facile electronic transport, thus active material-to-binder interactions need to be revised from existing designs. Specifically, polar functional groups that are useful in creating strong supramolecular interactions with bare Si are not adaptable to the hydrophobic carbon surface.

Y. Cho, J. Kim, Dr. S. Choi, K. Park, Prof. K. Char, Prof. J. W. Choi
School of Chemical and Biological Engineering
and Institute of Chemical Processes
Seoul National University
1 Gwanak-ro, Gwanak-gu, Seoul 08826, Republic of Korea
E-mail: khchar@snu.ac.kr; jangwookchoi@snu.ac.kr

A. Elabd, Prof. A. Coskun
Department of Chemistry
University of Fribourg
Chemin de Musee 9, Fribourg 1700, Switzerland
E-mail: ali.coskun@unifr.ch

Dr. T.-w. Kwon
Graduate School of Energy, Environment, Waterm,
and Sustainability (EEWS)
Korea Advanced Institute of Science and Technology (KAIST)
291 Daehak-ro, Yuseong-gu, Daejeon 34141, Republic of Korea
Dr. Jungmin Lee
Samsung SDI R&D Center
130 Samsung-ro, Yeongtong-gu, Suwon
Gyeonggi-do 16678, Republic of Korea

On another note, supramolecular chemistry has been recognized as a useful tool box in designing polymeric binders for Si electrodes.^[11] The rationale behind was that strong reversible bonding via noncovalent interactions can recover active material-to-binder interaction even when the original interaction is lost due to the volume expansion of Si. Thus, supramolecular interactions constitute the basis for self-healing mechanism that is critical in maintaining the mechanochemical integrity of Si electrodes. Besides the self-healing mechanism, mechanically interlocked molecules in the form of rotaxanes, in which the dynamic nature of supramolecular interactions is fully preserved, can endow high elasticity to buffer the volume change of Si, even in the microparticle cases, and polyrotaxane (PR) cross-linked poly(acrylic acid) (PAA) binder represents such an opportunity.^[10] In the PR, the ring components can move freely along the thread while being crosslinked to PAA network, which imparts extraordinary stretchability (>400%) to the entire polymer network. This pulley-like operation bearing PR effectively dissipates the stress in the Si electrode.

In an effort to utilize the useful design principles involving supramolecular chemistry, particularly the ring-sliding motion of polyrotaxanes for current commercial active materials, we adopted polyrotaxane-containing binder, namely, PRPAA, for SiO_x electrodes. To facilitate the active material-to-binder interaction for carbon-coated SiO_x (c-SiO) particles, we took advantage of noncovalent functionalization of the hydrophobic carbon coating surface by attaching a hydroxylated pyrene derivative.^[12] While the pyrene moiety enables strong π - π stacking interactions with the carbon surface, hydroxyl moiety facilitates hydrogen bonding interactions with the PRPAA. Notably, this approach functionalizes the surface of c-SiO without altering the electrical properties of carbon coating layer. While the pyrene treatment solely improves the particle-to-particle interaction and the electrode-to-current collector adhesion dramatically, the addition of PRPAA further improves the cycling performance even at commercial levels of areal capacity (≈ 3 mAh cm⁻²) in pairing with state-of-the-art cathode material (LiNi_{0.8}Co_{0.15}Al_{0.05}O₂ (NCA)) with high loadings (19–28 mg cm⁻²) by utilizing its high elasticity. The present study represents the promise of supramolecular chemistry in tuning the interparticle interaction in the emerging high capacity battery electrodes.

Figure 1a illustrates the surface modification of c-SiO with 1-pyrenemethanol (PyOH). While various binders incorporating polar adhesive functional groups are generally adopted for Si electrodes, these binders are not feasible for pristine c-SiO due to the hydrophobic carbon surface layer that is essential to compensate for the low electronic conductivity of SiO_x. The interaction of c-SiO with PAA binder must be mainly through weak Van der Waals interactions (Figure 1a). Moreover, it could be difficult to disperse c-SiO within the polar binder network due to strong hydrogen bonding interactions between the PAA chains. When c-SiO is treated with PyOH, however, the hydroxyl group on PyOH sticks out upon adsorption of pyrene moiety onto the conjugated carbon surface of c-SiO through π - π interaction, constituting PyOH-c-SiO assembly, namely, Py-c-SiO. The hydroxyl groups in this assembly enable strong hydrogen bonds with both PAA and other Py-c-SiO particles, enhancing the structural integrity of the entire Py-c-SiO electrode. Furthermore, PRs can be crosslinked to PAA to impart

elasticity to the PAA binder network as displayed in Figure 1b and thus substantially improve the mechanical stability of the SiO_x electrode. The high stretchability and resilience of the PRPAA network arise from the sliding motion of cyclodextrin (CD) rings threaded on the poly(ethylene glycol) (PEG) chain while the CD rings are covalently crosslinked to PAA through an ester linkage. The elasticity of the binder network endows the electrode with the ability of accommodating the volume change of active material by binder's "breathing" in harmony with the active material.

To see the possibility of the surface functionalization with PyOH, bare c-SiO particles were analyzed by transmission electron microscopy (TEM) (Figure 2a). As clearly shown in the magnified view, carbon layered structure was observed on the outer surface of c-SiO. The fast Fourier transform (FFT) pattern of the magnified view was circular, whose ring diameter corresponds to *d*-spacing of 3.4 Å, indicating that the carbon surface layer consists of graphitic carbon material (Figure 2a, inset). This carbon configuration is ideal for supramolecular functionalization through strong π - π stacking interactions. Elemental mapping via energy dispersive spectroscopy (EDS) reveals a consistent result such that carbon was detected around c-SiO particles (Figure S1, Supporting Information). The surface modification of c-SiO with PyOH was carried out in dimethyl sulfoxide (DMSO) solution of PyOH by a simple stirring process under ambient conditions. The effect of the PyOH functionalization on the surface properties of c-SiO was reflected in water contact angle measurements (Figure 2b). The contact angle of 5 μ L water droplet on pristine c-SiO pellet was 124°, verifying the hydrophobic nature of the c-SiO surface. By contrast, the Py-c-SiO pellet exhibited 74° owing to the polar hydroxyl group of PyOH.

The amount of PyOH adsorbed on c-SiO was estimated by UV-vis analysis (Figure 2c). The absorbance of the PyOH solution at 346 nm, a characteristic wavelength for PyOH, decreased by 2.2% after the surface modification with PyOH. Using the Beer-Lambert law, the amount of adsorbed PyOH was found to be ≈ 5 mg g⁻¹ of c-SiO, corresponding to 0.5 wt% of active material. A control test with 1-naphthalenemethanol with a lower degree of conjugation yielded less adsorption with c-SiO (Figure S2, Supporting Information), indicating the importance of substantial π electrons in the coating material for the π - π interaction on the surface of c-SiO.

In spite of the relatively small amount of adsorbed PyOH, the PyOH functionalization brought a substantial influence on the adhesion strength of the electrode (Figure 2d). When tested using the so-called 180° peeling method, in which the adhesion force was monitored with varying displacement of peeling tape, the Py-c-SiO electrode with 10 wt% PAA showed approximately four times as high average adhesion force as the bare c-SiO electrode counterpart with the same amount of PAA along the displacement of 10–20 mm: 16.65 versus 3.86 g_f mm⁻¹. The increased adhesion strength of the Py-c-SiO electrode is attributed to the hydrogen bond interaction between Py-c-SiO and PAA. Notably, the enhanced adhesion property of Py-c-SiO-PAA was preserved even during electrochemical cycling where the electrode was in contact with the electrolyte (Figure S3, Supporting Information). When polyethylene (PE) separators were retrieved after 60 cycles of half-cell operation, PE separator from c-SiO-PAA had more electrode debris than that

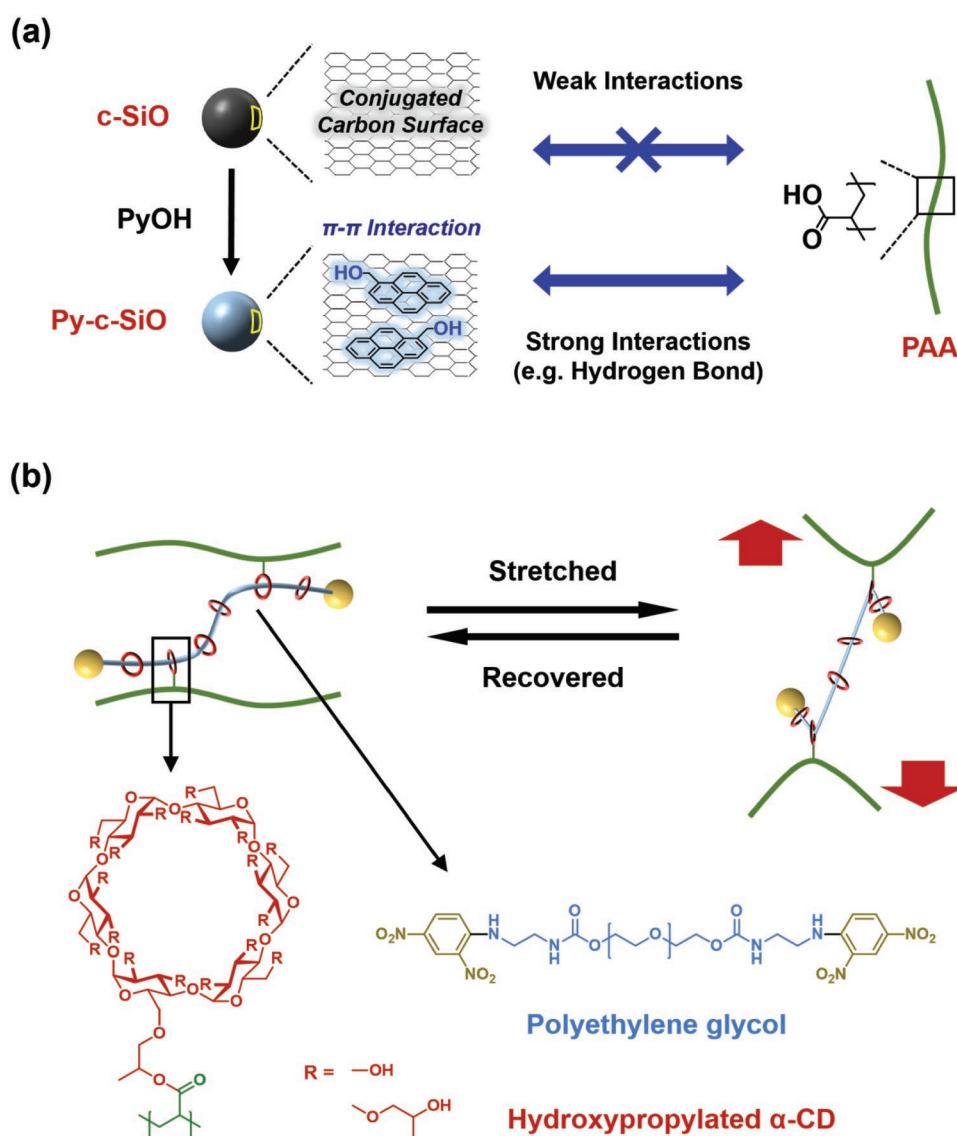


Figure 1. a) Schematic illustration of surface modification of c-SiO using PyOH and its interaction with PAA. b) Graphical representation depicting ring-sliding motion in PRPAA and its chemical structure.

of Py-c-SiO-PAA, which reflects the stronger interparticle interaction of Py-c-SiO-PAA. In addition, when the Py-c-SiO-PAA electrode was immersed in 5 mL of the ethylene carbonate (EC)/diethylene carbonate (DEC) electrolyte for 1 d, PyOH was not detected at all from the EC/DEC electrolyte, indicating that PyOH in the electrode does not dissolve into the electrolyte.

Based on the enhanced adhesion by integrating PyOH and to improve the mechanical properties of the electrode, PRPAA was also employed as a binder to take advantage of its high elasticity compared to PAA. The Py-c-SiO electrode with PRPAA is denoted as Py-c-SiO-PRPAA. Notably, PyOH, PAA, and PRPAA were all soluble in DMSO (Figure S4, Supporting Information). The electrochemical performances of all electrodes were evaluated under galvanostatic charging–discharging protocol in the form of coin-type Li half-cells in the potential range of 0.01–1.5 V versus Li/Li⁺. Each electrode consists of active material, binder, and conductive agent (Super P, Timcal, Switzerland) in a

weight ratio of 8:1:1. The initial coulombic efficiencies (ICEs) of the c-SiO-PAA, Py-c-SiO-PAA, and Py-c-SiO-PRPAA electrodes were 70.68%, 71.74%, and 75.52%, respectively, pointing to the fact that the high elasticity of binder and the strengthened particle-to-particle contacts by the supramolecular surface functionalization improve the interfacial stability.^[10,11] It is noted that the ICE values of these electrodes are not highly competitive for practical adoption due to the intrinsic material features of the used SiO_x related to Li ion trapping, oxygen anion mobility, etc. The values would be increased substantially by using advanced SiO_x analogs that incorporate foreign atom doping and Si domain control.^[13]

Cycling performance and corresponding CEs displayed a consistent trend among the samples (Figure 3a,b) when evaluated at an initial areal capacity at around 3 mAh cm⁻², a comparable value to those of commercial cells. The Py-c-SiO-PAA electrode showed clearly better capacity retention compared to

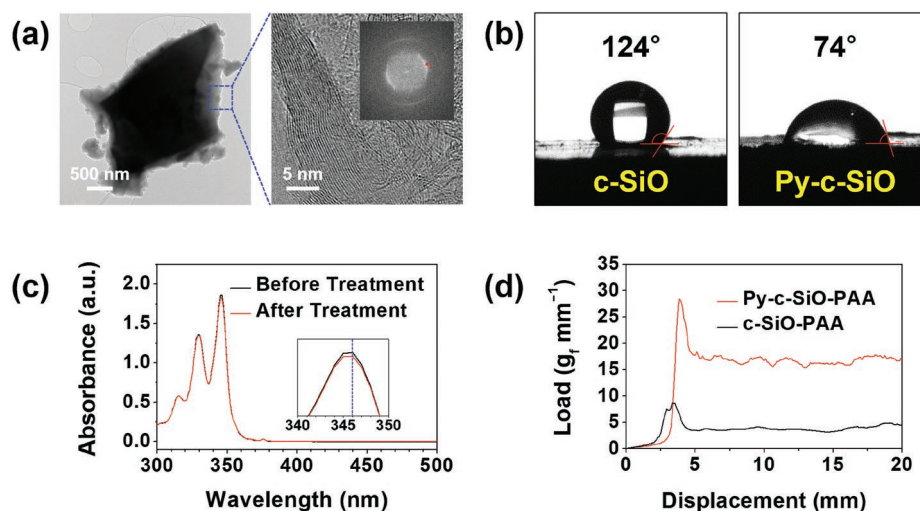


Figure 2. a) TEM images and fast Fourier transform (FFT) pattern of c-SiO. b) Water contact angle measurements of c-SiO pellet without and with the PyOH functionalization. c) UV-vis spectra of diluted 0.1 M PyOH solution before and after the c-SiO modification. d) 180° peeling test profiles of c-SiO-PAA and Py-c-SiO-PAA electrodes.

that of the c-SiO-PAA electrode, as the Py-c-SiO-PAA electrode maintained the capacity until it decayed at around 60th cycle whereas the capacity of the c-SiO-PAA electrode decayed tangibly from the beginning. The more sustainable operation of the Py-c-SiO-PAA electrode is ascribed to its improved particle-to-particle cohesion and electrode-to-current collector adhesion via the hydrogen bonding interaction involving PyOH. By contrast, the Py-c-SiO-PRPAA electrode preserved an areal capacity of 2.54 mAh cm⁻² even after 100 cycles operated at 0.5 C, corresponding to 97.6% capacity retention with respect to the value at the first cycle. The average CEs of the c-SiO-PAA, Py-c-SiO-PAA, and Py-c-SiO-PRPAA electrodes for the first 30 cycles after one precycle were 99.08%, 99.25%, and 99.38%, respectively. Remarkably, the CE of Py-c-SiO-PRPAA increased rapidly from the beginning and reached 99.11%, 99.70%, and 99.73% at the 5th, 20th, and 30th cycles (Figure 3b), respectively, revealing its superior interface stability. In order to see the impact of the surface functionalization with PyOH more directly, unmodified c-SiO was integrated with PRPAA and tested under the same conditions. Remarkably, even though PRPAA was used, the c-SiO-PRPAA electrode showed rapid capacity fading only after the 50th cycle (Figure S5, Supporting Information), pointing to the weak interactions between PRPAA and bare c-SiO due to the hydrophobic nature of the c-SiO surface.

Based on the promising cycling performance of the Py-c-SiO-PRPAA electrode for 100 cycles, the test was extended for additional 350 cycles to cover total 450 cycles (Figure 3c). The capacity retentions at the 150th, 200th, and 250th cycles were 99.6%, 97.9%, and 92.6%, respectively. The average CE in the cycling period of 30–250 was 99.83%. Since we suspected the degradation of Li metal counter electrode as the origin of capacity fading after the 250th cycle, Li counter electrode was replaced with a fresh one at the 310th cycle. Upon this replacement, we observed that the areal capacity was restored nearly to the initial capacity in the very beginning of cycling and sustained until the 450th cycle without a critical capacity drop, verifying highly robust nature of the Py-c-SiO-PRPAA electrode based on the synergistic effect between PyOH and PRPAA.

In an attempt to investigate the kinetics of all electrodes during charge–discharge, a rate capability test was conducted. When C-rate was varied from 0.1 to 2 C, the Py-c-SiO-PRPAA electrode exhibited higher capacity retentions compared to those of the other two electrodes (Figure 3d). Consistent with the cycling test in Figure 3a, the c-SiO-PAA electrode suffered from capacity fading over repeated rounds of C-rate variation. The superior rate performance of the Py-c-SiO-PRPAA electrode can be explained by its compact contacts between electrode components that facilitate Li ion transport. Cyclic voltammetry (CV) profiles at various scan rates afforded more detailed information on the electrode kinetics (Figure S6, Supporting Information). For this analysis, the cathodic peak currents (I_{pc}) from various scan rates (ν) were logarithmically plotted (Figure 3e) following the power-law relation: $I_{pc} = a\nu^b$. The b value, which corresponds to the slope of $\log I_{pc}$ versus $\log \nu$ plot, is known to be correlated to Li-ion diffusion kinetics within the electrode, and higher b value implies faster electrochemical reaction.^[14] The Py-c-SiO-PRPAA electrode showed higher b value of 0.58 compared to that of the Py-c-SiO-PAA electrode (0.55), reconfirming the useful role of PyOH and PRPAA in the rate capability. Electrochemical impedance spectroscopy (EIS) measurements also showed consistent results (Figure S7, Supporting Information). Both semicircles of the Nyquist plot of the Py-c-SiO-PRPAA electrode were smaller than those of the Py-c-SiO-PAA counterpart, indicating lower SEI resistance (R_{SEI}) and charge transfer resistance (R_{ct}).^[14b,15] Supplementary CV tests with only PAA, PRPAA, and PyOH demonstrated the electrochemical stability of these components in the given range of operation potential (Figure S8, Supporting Information).

Based on the encouraging results of the Py-c-SiO-PRPAA electrode in half-cells, tests were expanded to full-cells paired with NCA cathode with a specific capacity of 190.5 mAh g⁻¹ at 0.05 C rate (Figure S9, Supporting Information). The n/p ratio defined as total anode capacity over total cathode capacity was set to 1.1. Figure 4a shows the initial charge–discharge profiles of full-cells with two different NCA mass loadings at 0.05 C

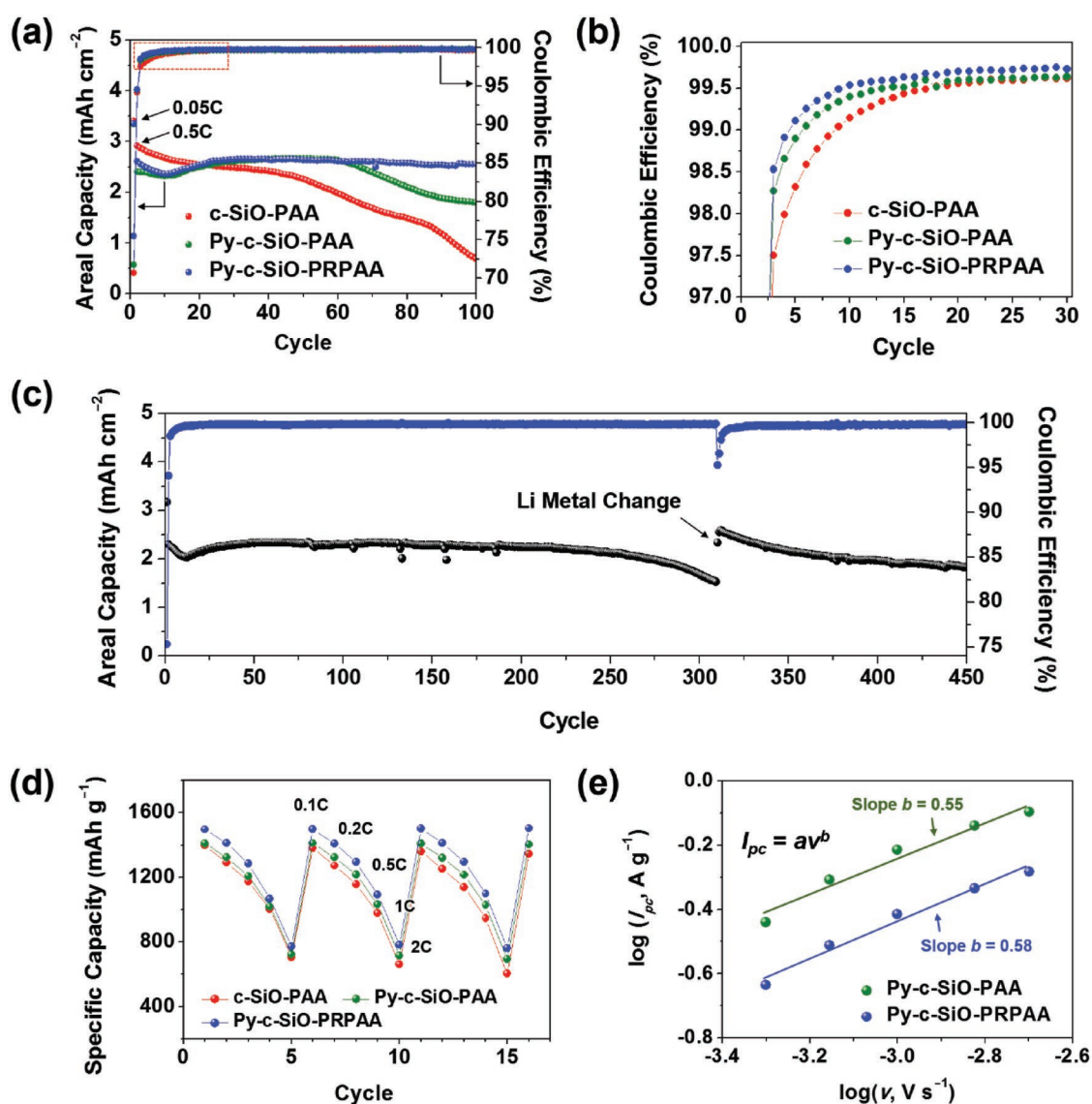


Figure 3. Electrochemical performance of Py-c-SiO electrodes based on PRPAA and PAA binders. a) Cycling performance of c-SiO-PAA (red), Py-c-SiO-PAA (green), and Py-c-SiO PRPAA (blue) electrodes measured at 0.5 C and b) their corresponding coulombic efficiencies in the first 30 cycles. c) Long-term cycling performance of Py-c-SiO-PRPAA electrode when measured at 0.5 C (1.78 mA cm⁻²). d) Rate capability at various C-rates. e) Plots of log (I_{pc}) versus log (v) from the cathodic peak currents of CV curves at various scan rates (v).

(green: 19.4 mg cm⁻²; black: 27.8 mg cm⁻²). These two different cathode loadings delivered discharging capacities of 2.79 and 4.03 mAh cm⁻², respectively, when measured at 0.05 C. In the case of the lower mass loading of NCA, capacity fading was moderate, as 82.5% of the original capacity was preserved after 150 cycles operated at 0.5 C (Figure 4b). Notably, the CE of this full-cell rose sharply such that the CE reached 99.9% at the 27th cycle and saturated above thereafter (see the inset of Figure 4b). In the case of the full-cell with the higher NCA loading, 3.13 mAh cm⁻² was maintained after 50 cycles under the same operation conditions. The decent cyclability of these two full-cells suggests that the synergy between PyOH and PRPAA works out well even in the commercial cell settings. It is noted that the performance is expected to improve further by additional optimization in cell fabrication and operation, such

as electrolyte additives. It also turned out that PyOH does not trigger hydrolysis of lithium hexafluorophosphate (LiPF₆) salt to damage the NCA cathode according to a control experiment with and without involving PyOH (Figure S10, Supporting Information). In the same line, additional transition metal dissolution was not detected from the separator of the PyOH-containing cell, verifying a negligible effect of PyOH to the NCA cathode (Figure S11, Supporting Information).

The substantially better cyclability of Py-c-SiO-PRPAA compared to that of its PAA-based counterpart is attributed to the resilience of PRPAA. See Figure S12 (Supporting Information) for the stress-strain curves of both binders. This distinct performance is schematically presented in Figure 5a. Although both electrodes start similarly in their pristine state in terms of distribution, upon repeated lithiation and delithiation, relatively

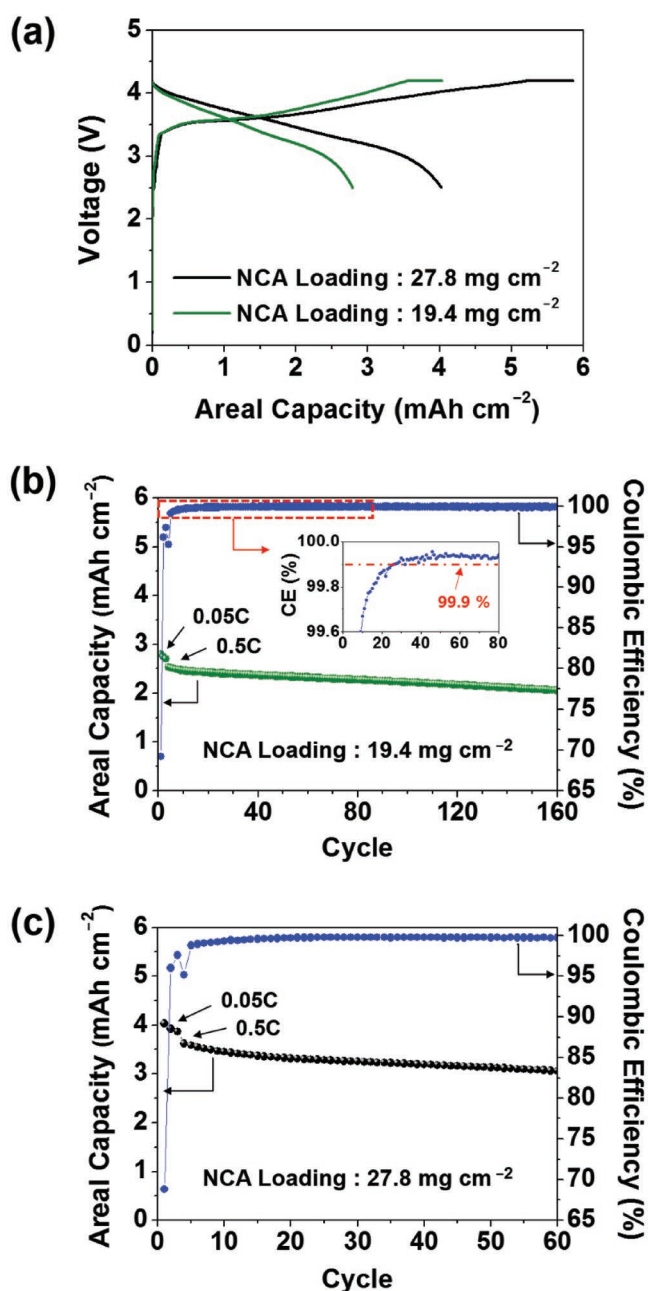


Figure 4. Electrochemical performance of full-cell based on Py-c-SiO-PRPAA electrode. a) Initial charge–discharge profiles of Py-c-SiO-PRPAA/LiNi_{0.8}Co_{0.15}Al_{0.05}O₂ full-cells with different active material loadings at 0.05 C and b,c) its cycling performance at 0.5 C, along with the coulombic efficiencies.

brittle PAA network is irreversibly deformed and eventually fractured by severe stress accumulation during the volumetric change of Py-c-SiO. This mechanical instability renders the electrode–electrolyte interface unstable from the chemistry viewpoint by an undesired electrolyte decomposition. By sharp contrast, the PRPAA network can largely avoid this issue as its resilience can recover the electrode integrity after delithiation by keeping electrode components tightly bound. This picture with regard to electrode stability was confirmed by scanning

electron microscopy (SEM) images of both electrodes during the course of precycling. In the case of the lithiated Py-c-SiO-PAA electrode, well-distributed super P and SEI layer were observed (Figure 5b,c), a typical phenomenon of Si electrodes after lithiation. However, traces of PAA were invisible. After delithiation, some cracks were observed throughout the electrode (Figure 5d). On the other hand, the lithiated Py-c-SiO-PRPAA electrode clearly showed traces of PRPAA (red dotted line in Figure 5e). These traces indicate the stretchability of PRPAA and its resulting conformal coverage of active particles. The stretched coverage was even more obvious from magnified SEM view (Figure 5f). The effect of high elasticity of PRPAA was reflected in uniform crack-free electrode morphology after precycle (Figure 5g).

Cross-sectional SEM analysis revealed the effect of binders more directly (Figure 6). Before cycling, both the Py-c-SiO-PAA and Py-c-SiO-PRPAA electrodes had the thickness of around 28 μm (Figure 6a,d). After precycle, however, both electrodes showed significant difference in their thickness in a way that the thickness of the Py-c-SiO-PAA electrode increased to 41 μm (Figure 6b), whereas that of the Py-c-SiO-PRPAA increased merely to 34 μm (Figure 6e). From a magnified SEM image (Figure 6c), it can be seen that the greater thickness increase of the Py-c-SiO-PAA electrode originated from a significant SEI growth between SiO_x particles, unlike the Py-c-SiO-PRPAA counterpart that maintained relatively compact interface between SiO_x particles. Thus, the high elasticity of PRPAA along with its improved interaction with the c-SiO through PyOH had a substantial effect on the swelling of c-SiO electrodes, a critical parameter in full-cell design and energy density, by stabilizing the SEI layer.

Supramolecular chemistry has received an increasing attention for binder design in emerging high capacity battery electrodes. The present study demonstrates such an opportunity by employing π - π stacking and hydrogen bonding interactions in surface modification and active material-to-binder connections, respectively. The incorporation of these two kinds of supramolecular interactions along with PRs improves the performance in cycle life, electrode adhesion, and electrode swelling mitigation compared to the case where either of those is involved, thus revealing the synergistic effect of supramolecular interactions. The current investigation also highlights the powerful and universal nature of polyrotaxane in keeping the electrode integrity via its high elasticity once its interaction with active material is warranted.

Experimental Section

Preparation of Py-c-SiO: PyOH was purchased from Sigma-Aldrich and used as received. 0.1 M PyOH solution was prepared in DMSO. 3 g of c-SiO powder (KSC1064, Shin-Etsu Chemical Co., Ltd) was added to 30 mL of the 0.1 M PyOH solution and stirred at room temperature for 2 d. The mixture was then filtered and washed with 30 mL of pure DMSO three times. The filtered Py-c-SiO powder was dried at 70 °C for 2 d right before its use.

Synthesis of PRPAA: PRPAA was synthesized following the previously reported procedures.^[10] Briefly, PEG ($M_w \approx 20k$) was activated through 1,1'-carbonyldiimidazole (CDI), and ethylenediamine was added to yield amine groups at both chain ends. Afterward, α -CD was threaded through PEG at an elevated temperature (80 °C), the generated amine groups

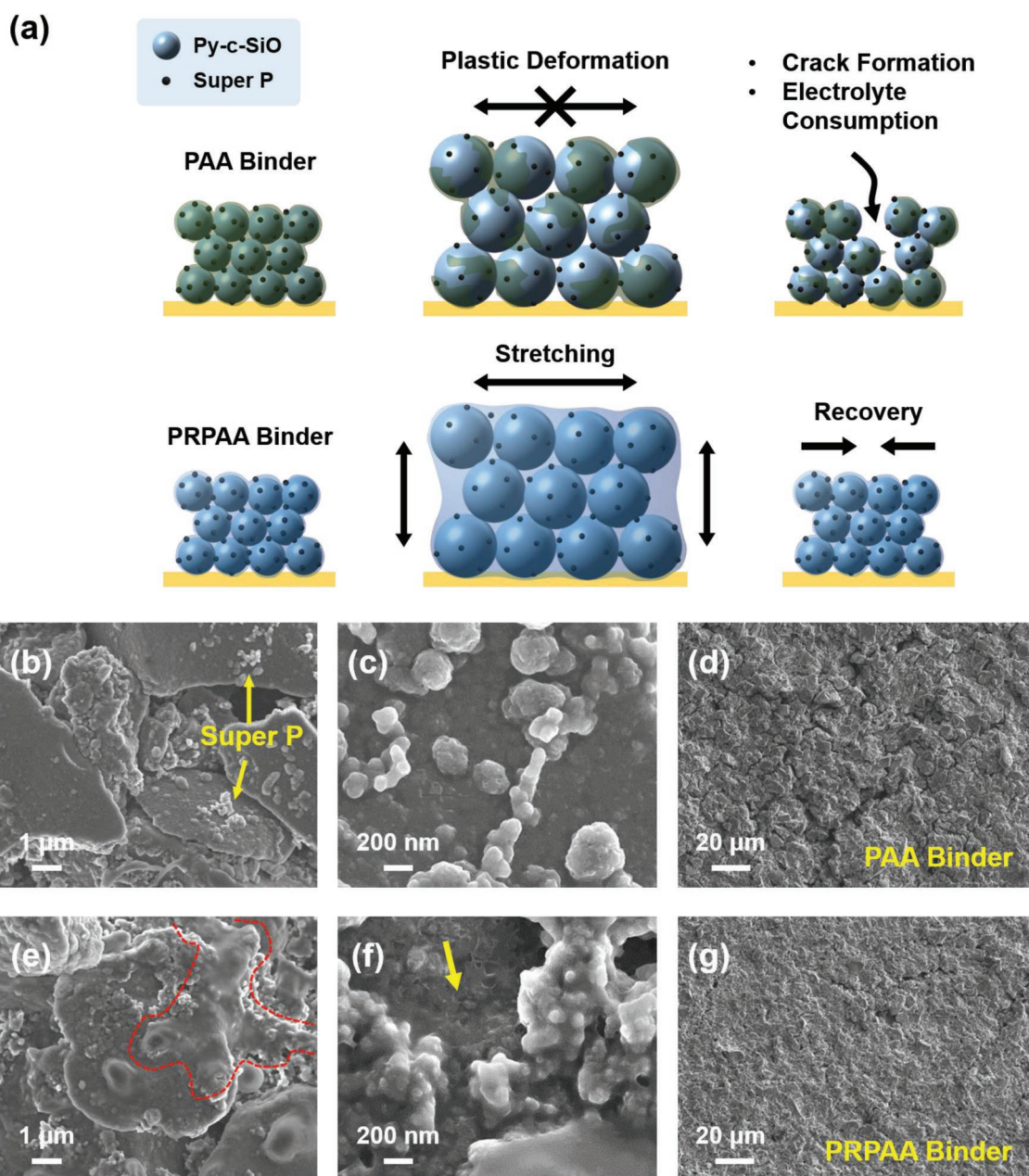


Figure 5. a) Schematic illustration of electrode structures during lithiation and delithiation. b,c) SEM images of Py-c-SiO-PAA electrode after the 1st lithiation. d) Top-view SEM image of Py-c-SiO-PAA after precycle. e,f) SEM images of Py-c-SiO-PRPAA electrode after the 1st lithiation. The red dotted line in (e) indicates stretched PRPAA binder on the active material. The arrow in (f) indicates stretched binder coverage over the electrode. g) Top-view SEM image of Py-c-SiO-PRPAA after precycle.

were capped with 2,4-dinitrofluorobenzene. Hydroxyl groups on the α -CD were partially reacted with propylene oxide to yield hydroxypropylated PR (HPR). Finally, PRPAA was obtained by crosslinking CDI-activated PAA ($M_w \approx 450\text{k}$) with hydroxyl groups on α -CD of HPR. The feed ratio of PAA to HPR was fixed at 95:5 in weight.

Material Characterization: The morphology characterization of active particles and EDS analyses were conducted using Cs-TEM (JEM-ARM200F, JEOL, Japan) and field-emission SEM (JSM-7600F, JEOL, Japan). X-ray diffraction analysis was performed using SmartLab (Rigaku, Japan). Contact angle measurements were conducted using DSA100 (Krüss, Germany) by dropping 5 μL deionized water on the surface of pelletized active materials. UV-vis spectra of the PyOH solutions were obtained using Lambda 35 (PerkinElmer, USA). For this

analysis, each PyOH solution (before and after c-SiO modification) was 2000-fold diluted. 180° peeling tests were conducted to evaluate adhesion strength using a universal testing machine (QM100S, QMESYS, South Korea). 3M double-sided tape (25 mm in width) was attached onto the electrodes and peeled off at a constant rate of 25 mm min^{-1} . Stress-strain curves of binder films were obtained using the same universal testing machine. Top-view and cross-section images of the electrodes were obtained using the aforementioned field-emission SEM and focused ion beam (Helios 650, FEI, USA) equipment, respectively. For the analysis of cycled electrodes, coin-cells were disassembled in an Ar-filled glove box. The electrodes were washed with EC/DEC (1/1 volume ratio), followed by drying under vacuum for 5 h.

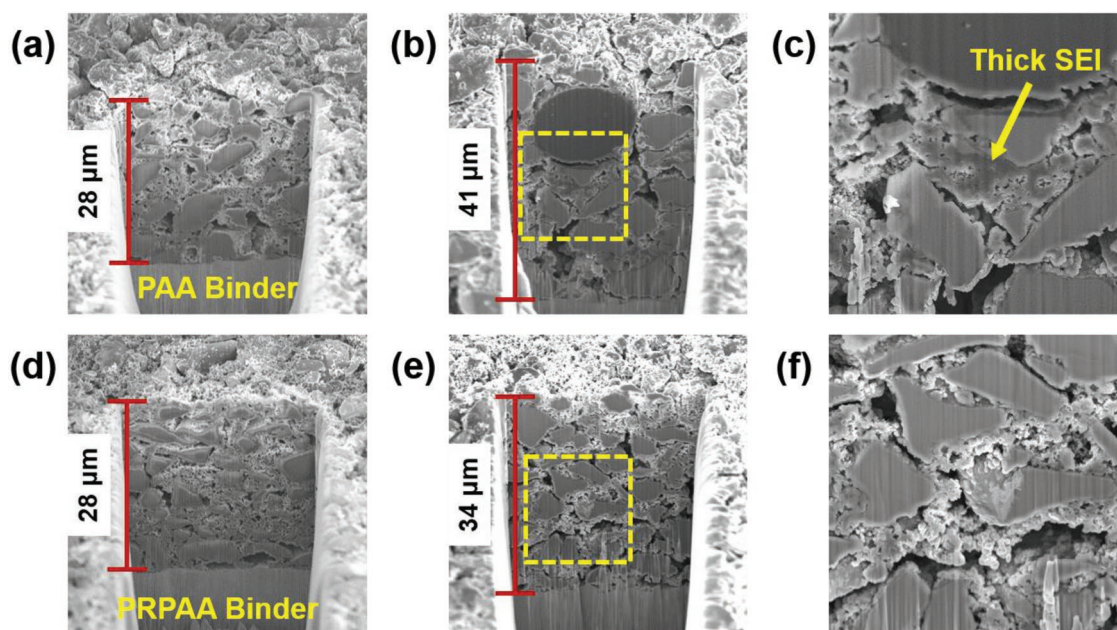


Figure 6. Cross-sectional SEM images of Py-c-SiO electrodes. a–c) The Py-c-SiO-PAA electrode in their pristine state (a) and after precycle (b,c). d–f) The Py-c-SiO-PRPAA electrode in their pristine state (d) and after precycle (e,f). (c) and (f) are magnified views from the boxes in (b) and (e).

Preparation of Electrodes: Mass loading of active material was between 2.3 and 2.5 mg cm⁻². For slurry preparation, active material, super P (Timcal, Switzerland), and binder were dispersed in DMSO at a weight ratio of 8:1:1. The slurry was cast on copper foil using the doctor blade method, followed by drying at 60 °C under vacuum overnight. The electrode was then compressed using a roll pressure to reach the density of 1.0–1.1 g cm⁻³. NCA cathode was prepared by dispersing NCA, super P, and polyvinylidene fluoride ($M_w \approx 534k$) in *N*-methyl-2-pyrrolidone at a weight ratio of 90:5:5. The slurry was cast on aluminum foil and dried at 60 °C under vacuum overnight.

Electrochemical Measurements: All electrochemical measurements were performed using CR2032 coin-type cells assembled in an Ar-filled glove box. For all cells, electrode diameters were 10 mm, and PE separator (SK Innovation, South Korea) was used. 1.0 M LiPF₆ in EC/DEC (1/1 volume ratio) containing 7.5 wt% fluoroethylenecarbonate and 0.5 wt% vinylene carbonate was used as electrolyte, and 100 μL of the electrolyte was injected to all cells tested in this study. Prior to cell tests, all cells were under rest for 6 h to ensure sufficient soaking of the electrolyte into the separator and electrodes. For cycling tests of Li half-cells, one precycle was preceded at 0.05 C before the rest of cycles scanned at 0.5 C in the potential range of 0.01–1.5 V versus Li/Li⁺. Each charge or discharge was processed at constant current (CC) mode using a battery cycler (WBCS 3000, WonAtech, South Korea). For rate capability tests, Li half-cells were precycled at 0.05 C for three times, and then scanned at various C-rates (0.1, 0.2, 0.5, 1.0, and 2.0 C). The full-cell tests were conducted in the potential range of 2.5–4.2 V. Three precycles at 0.05 C were processed under constant current constant voltage (CCCV) mode for charging and CC mode for discharging. Subsequent cycles were also cycled under CCCV mode for charging and CC mode for discharging at 0.5C. EIS measurements were performed using a potentiostat (VSP, Bio-Logic, France) over frequency range from 1 MHz to 0.1 Hz. CV analysis was conducted for kinetic study at a series of scan rates (0.5, 0.7, 1.0, 1.5, and 2.0 mV s⁻¹) in the potential range of 0.01–1.5 V versus Li/Li⁺.

Supporting Information

Supporting Information is available

Acknowledgements

Y.C., J.K., and A.E. contributed equally to this work. The authors acknowledge financial support from the National Research Foundation of Korea (Grant No. NRF-2018R1A2A1A19023146). This work was also supported by Samsung SDI.

Conflict of Interest

The authors declare no conflict of interest.

Keywords

cyclodextrin, molecular machines, polyrotaxanes, pyrene, swelling

- [1] a) J. W. Choi, D. Aurbach, *Nat. Rev. Mater.* **2016**, *1*, 16013; b) S. Chae, M. Ko, K. Kim, K. Ahn, J. Cho, *Joule* **2017**, *1*, 47.
- [2] a) C. K. Chan, H. Peng, G. Liu, K. McIlwrath, X. F. Zhang, R. A. Huggins, Y. Cui, *Nat. Nanotechnol.* **2008**, *3*, 31; b) A. Magasinski, P. Dixon, B. Hertzberg, A. Kvit, J. Ayala, G. Yushin, *Nat. Mater.* **2010**, *9*, 353; c) S. Chen, M. L. Gordin, R. Yi, G. Howlett, H. Sohn, D. Wang, *Phys. Chem. Chem. Phys.* **2012**, *14*, 12741; d) X. H. Liu, L. Zhong, S. Huang, S. X. Mao, T. Zhu, J. Y. Huang, *ACS Nano* **2012**, *6*, 1522.
- [3] a) M. Zhou, M. L. Gordin, S. Chen, T. Xu, J. Song, D. Lv, D. Wang, *Electrochem. Commun.* **2013**, *28*, 79; b) S. Kim, Y. K. Jeong, Y. Wang, H. Lee, J. W. Choi, *Adv. Mater.* **2018**, *30*, 1707594; c) Z. Liu, Q. Yu, Y. Zhao, R. He, M. Xu, S. Feng, S. Li, L. Zhou, L. Mai, *Chem. Soc. Rev.* **2019**, *48*, 285.

- [4] a) Y. Shi, X. Zhou, G. Yu, *Acc. Chem. Res.* **2017**, *50*, 2642; b) J. Lopez, D. G. Mackanic, Y. Cui, Z. Bao, *Nat. Rev. Mater.* **2019**, *4*, 312.
- [5] a) J. Guo, C. Wang, *Chem. Commun.* **2010**, *46*, 1428; b) B. Koo, H. Kim, Y. Cho, K. T. Lee, N.-S. Choi, J. Cho, *Angew. Chem., Int. Ed.* **2012**, *51*, 8762; c) H. Wu, G. Yu, L. Pan, N. Liu, M. T. McDowell, Z. Bao, Y. Cui, *Nat. Commun.* **2013**, *4*, 1943; d) B. Liu, P. Soares, C. Checkles, Y. Zhao, G. Yu, *Nano Lett.* **2013**, *13*, 3414; e) J. Song, M. Zhou, R. Yi, T. Xu, M. L. Gordin, D. Tang, Z. Yu, M. Regula, D. Wang, *Adv. Funct. Mater.* **2014**, *24*, 5904.
- [6] a) N. S. Hochgatterer, M. R. Schweiger, S. Koller, P. R. Raimann, T. Wöhrle, C. Wurm, M. Winter, *Electrochem. Solid-State Lett.* **2008**, *11*, A76; b) I. Kovalenko, B. Zdyrko, A. Magasinski, B. Hertzberg, Z. Milicev, R. Burtovyy, I. Luzinov, G. Yushin, *Science* **2011**, *334*, 75; c) C.-H. Jung, K.-H. Kim, S.-H. Hong, *ACS Appl. Mater. Interfaces* **2019**, *11*, 26753.
- [7] a) A. Magasinski, B. Zdyrko, I. Kovalenko, B. Hertzberg, R. Burtovyy, C. F. Huebner, T. F. Fuller, I. Luzinov, G. Yushin, *ACS Appl. Mater. Interfaces* **2010**, *2*, 3004; b) Y. K. Jeong, T.-w. Kwon, I. Lee, T.-S. Kim, A. Coskun, J. W. Choi, *Nano Lett.* **2014**, *14*, 864.
- [8] a) T.-w. Kwon, Y. K. Jeong, I. Lee, T.-S. Kim, J. W. Choi, A. Coskun, *Adv. Mater.* **2014**, *26*, 7979; b) Y. K. Jeong, T.-w. Kwon, I. Lee, T.-S. Kim, A. Coskun, J. W. Choi, *Energy Environ. Sci.* **2015**, *8*, 1224.
- [9] a) C. Wang, H. Wu, Z. Chen, M. T. McDowell, Y. Cui, Z. Bao, *Nat. Chem.* **2013**, *5*, 1042; b) T.-w. Kwon, Y. K. Jeong, E. Deniz, S. Y. AlQaradawi, J. W. Choi, A. Coskun, *ACS Nano* **2015**, *9*, 11317; c) C. Luo, X. Fan, Z. Ma, T. Gao, C. Wang, *Chem* **2017**, *3*, 1050; d) Z. Xu, J. Yang, T. Zhang, Y. Nuli, J. Wang, S.-i. Hirano, *Joule* **2018**, *2*, 950; e) G. Zhang, Y. Yang, Y. Chen, J. Huang, T. Zhang, H. Zeng, C. Wang, G. Liu, Y. Deng, *Small* **2018**, *14*, 1801189; f) Y. K. Jeong, J. W. Choi, *ACS Nano* **2019**, *13*, 8364.
- [10] S. Choi, T.-w. Kwon, A. Coskun, J. W. Choi, *Science* **2017**, *357*, 279.
- [11] a) T.-w. Kwon, J. W. Choi, A. Coskun, *Chem. Soc. Rev.* **2018**, *47*, 2145; b) T.-w. Kwon, J. W. Choi, A. Coskun, *Joule* **2019**, *3*, 662.
- [12] S. Srinivasan, W. H. Shin, J. W. Choi, A. Coskun, *J. Mater. Chem. A* **2013**, *1*, 43.
- [13] a) M. Miyachi, H. Yamamoto, H. Kawai, *J. Electrochem. Soc.* **2007**, *154*, A376; b) J.-I. Lee, K. T. Lee, J. Cho, J. Kim, N.-S. Choi, S. Park, *Angew. Chem., Int. Ed.* **2012**, *51*, 2767; c) H. J. Kim, S. Choi, S. J. Lee, M. W. Seo, J. G. Lee, E. Deniz, Y. J. Lee, E. K. Kim, J. W. Choi, *Nano Lett.* **2016**, *16*, 282.
- [14] a) Y. Tao, Y. Wei, Y. Liu, J. Wang, W. Qiao, L. Ling, D. Long, *Energy Environ. Sci.* **2016**, *9*, 3230; b) Y. H. Kwon, K. Minnici, S. R. Lee, G. Zhang, E. S. Takeuchi, K. J. Takeuchi, A. C. Marschilok, E. Reichmanis, *ACS Appl. Energy Mater.* **2018**, *1*, 2417; c) X. Yang, A. L. Rogach, *Adv. Energy Mater.* **2019**, *9*, 1900747.
- [15] S.-H. Park, H. J. Kim, J. Lee, Y. K. Jeong, J. W. Choi, H. Lee, *ACS Appl. Mater. Interfaces* **2016**, *8*, 13973.